Supplementary Information (SI) for Nanoscale.
This journal is © The Royal Society of Chemistry 2025

# High-Performance All-Inorganic CdSe/CdS Nanorod-based Light Emitting Diodes Enabled by Controlled Electrophoretic Deposition

Nandita Biswas, Anthony Mullen, Lin Lyu, Yongliang Zhang, Charlie O'Mahony, Matthew Snelgrove, Sergey Beloshapkin, Devika Laishram, Jinlei Wu, Syed A. M. Tofail, Christophe Silien, Kevin M. Ryan and Ning Liu

## Supplementary Information

Table S1: Summary of NR-LED performance

| Nanorod | PLQY in film (%) | Max luminescence ($Cd/m^2$) | EQE (%) | Method | Structure | | Ref |
|---|---|---|---|---|---|---|---|
| CdSe/CdS/CdS | 72 | 104000 | 15.7 | Spin coating | Hybrid | ITO/PEDOT:PSS/TFB/NRs/PMMA/ZnO/Al | 1 |
| CdSe/CdS | 30-42 | 42300 | 8.4 | Spin coating | Hybrid | ITO/(PEDOT:PSS)/PVK/QR/ZnMgO/Al | 2 |
| CdSe/CdS | 44 | 3960 | 7 | Spin coating | Hybrid | ITO/PEDOT:PSS/PVK/QRs/PMMA/ZnO/LiF/Al | 3 |
| CdSe/CdS | 90 | 50000 | 18 | Spin coating | Hybrid | ITO/ZnO/NRs/spiro-2NPB-9/9-spirobifluorene/LT-N125/LG-101/Al | 4 |
| CdSe/CdS/ZnS | 40 | 76000 | 12 | Spin coating | Hybrid | ITO/PEDOT:PSS/TFB/$F_4$TCNQ/NRs/ZnO/Al | 5 |
| CdSe/CdS | NA | 4320 | 6.3 | EPD | Hybrid | ITO/ZnO/NRs/PVK/TFB/Au | 4 |
| CdSe/CdS | 55 | 3290 | 1.2 | EPD | All-Inorganic | ITO/ZnO/NRs/NiMgO/Au | 5 |
| CdSe/CdS | 35-40 | 1735 | 10.8 | EPD | All-Inorganic | ITO/$NiO_x$/PF-BT/NRs/ZnMgO/Ag | This work |

1. Y. B. Zhang, F. J. Zhang, H. Z. Wang, L. Wang, F. F. Wang, Q. L. Lin, H. B. Shen, and L. S. Li, *Optics express*, 2019, **27**, 7935-7944.
2. M. Kumar, M. F. Prodanov, Z. B. Liao, C. B. Kang, J. X. Song, D. Bhadra, R. R. Gavara, and A. K. Srivastava, *Nano Research*, 2025, **18**, 94907071.
3. M. Kumar, M. F. Prodanov, C. Dezhang, M. Marus, C. B. Kang, S. B. Shivarudraiah, V. V. Vashchenko, J. E. Halpert, and A. K. Srivastava, *ACS Applied Materials & Interfaces*, 2022, **14**, 18723-18735.
4. B. S. Mashford, M. Stevenson, Z. Popovic, C. Hamilton, Z. Q. Zhou, C. Breen, J. Steckel, V. Bulovic, M. Bawendi, S. Coe-Sullivan, P. T. Kazlas, *Nature photonics*, 2013, **7**, 407-412.
5. S. Nam, N. Oh, Y. Zhai, M. Shim, *ACS nano*, 2015, **9**, 878-885.
6. Y. L. Zhang, X. M. Pham, T. Keating, N. Jia, A. Mullen, D. Laishram, M. Y. Gao, ACS Applied Materials & Interfaces, 2024, **16**, 10459-10467.
7. Y. L. Zhang, N. Jia, D. Laishram, K. H. Shah, L. Lyu, M. Y. Gao, P. Liu, *ACS Applied Nano Materials*, 2024, **7**, 23617-23626.

## Coupled rate equations for EPD of nanoparticles from solution

In addition to the equations discussed in the main texts, if we assume the charged NPs become neutral before some of them re-dissolve back to the solution, we can also add eq. (S5) and (S6) to calculate the concentration of the neutral particles as well as the total particle concentration as a function of time:

$$\begin{cases} \frac{dw}{dt} = R_{dep} - R_{dis} & (S1) \\ R_{dep} = Im/q & (S2) \\ I = \frac{c_c v A q}{m} & (S3) \\ c_c = c_0 - \frac{\int R_{dep} dt}{V} & (S4) \\ c_n = \frac{\int R_{dis} dt}{V} & (S5) \\ c = c_c + c_n & (S6) \end{cases}$$

Here $c_n$ indicates the concentration of neutral NPs and $c$ the concentration of total NPs in solution. If we assume the CdSe/CdS core-shell NRs having a core diameter of 4 nm and overall size of 6 nm × 15 nm, the mass of single NR is $2.08\times10^{-21}$ kg. If we use the effective radius to approximate the NR, assuming the sphere having the same mass as the NR, the equivalent $r$ = 10 nm. If we further assume a deposition area of 1.8 cm$^2$, a solution volume of 18 ml, the viscosity of Toluene 5.54 $\times10^{-4}$ Pa·s, and an electric field of 160 V/mm, we can calculate the NP velocity in the solution as discussed in ref [23] of the main text:

$$v = \frac{qE}{6\pi r\eta}\left(1 - \exp\left(-\frac{6\pi r\eta t}{m}\right)\right) \qquad (S7)$$

Figure S1 below shows the velocity of NPs in solution reaching its steady state value in less than a few tenths of a nanosecond. The steady state velocity is proportional to the charge of the particles in solution.

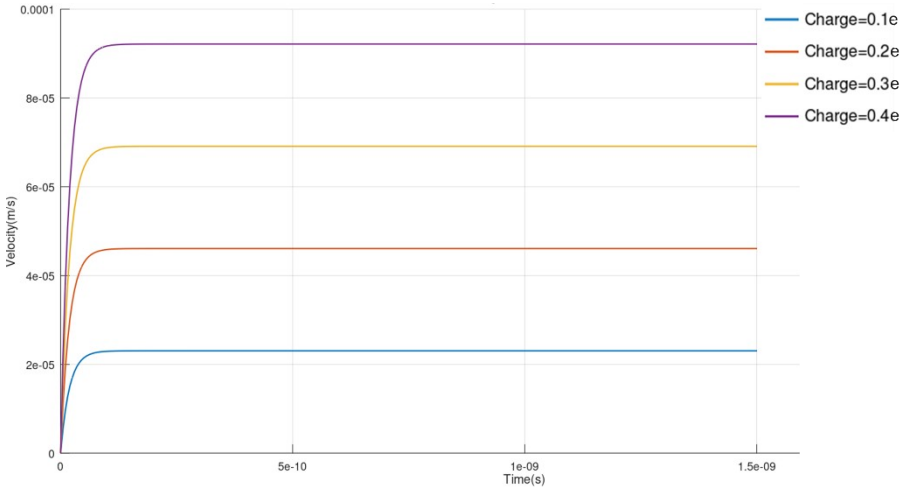


**Figure S1**: Velocity of NPs in Toluene carrying different charges in terms of electron charge e.

**Numerical modelling of the coupled equations**

Apart from the analytical approximation we demonstrated in the main texts, we also numerically modelled the current, deposition rate and changes in the charged particle concentration as well as the

deposited mass by charged particle as a function of time following eq. (S1) to (S4) using an initial NP concentration of 5 mg/ml, without considering $R_{dis}$, since we consider $R_{dis}$ is only associated with the neutral particles and the current I is only related to charged particles. The parameters used for Figure S2 simulations are the same as for Figure S1. It is clear that the limited volume of NP solution can impact the deposition significantly.

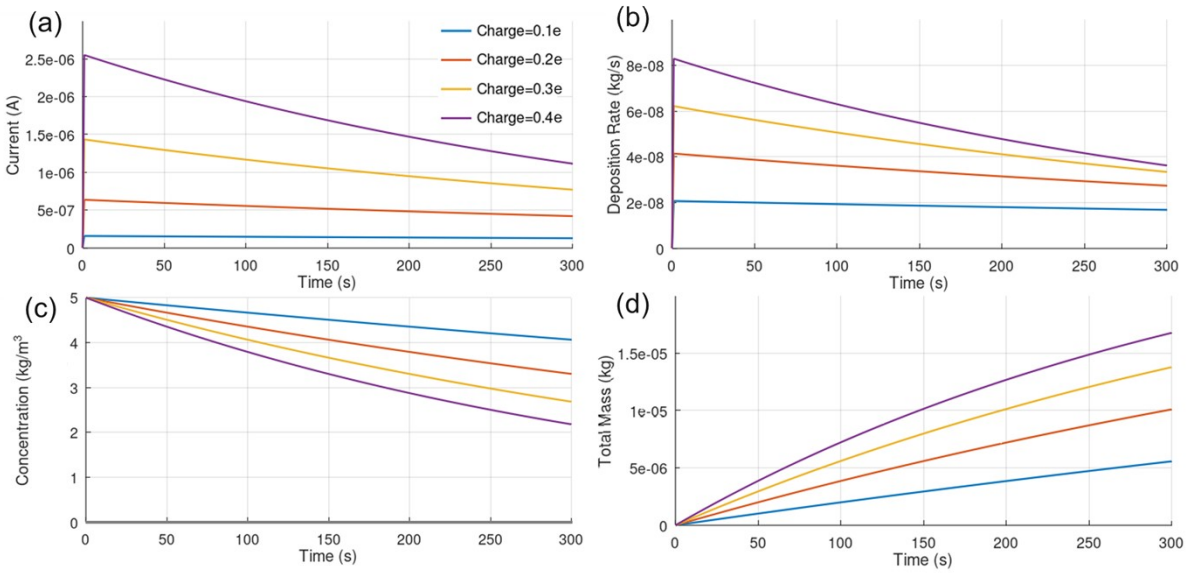


**Figure S2**: Modelling of $I$, $R_{dep}$, $c_c$ and $w$ vs. time with an initial charged NP $c_0$= 5 mg/ml

Our numerical model and analytical approaches are consistent with each other. As discussed in the main texts, we can obtain the single particle charge $q$ from the single exponential decay fitting to the I-t curve, such as EPD1. The NRs used for EPD1 and EPD2 are 6 nm × 38 nm, with an effective $r$ = 13.6 nm, deposition area of 0.9 cm$^2$, a NR solution volume of 6 ml and an initial NR concentration of 15 mg/ml. The fitting to EPD1 yields a single particle charge of 0.3 ± 0.02 e, consistent with the ones reported in the literature.

**Dissolution of NRs**

The deposited mass calculated from Figure S2 (d) is > 20 times larger than what we measured post-experiments using SEM. This significant discrepancy can only be explained by a large dissolution rate $R_{dis}$ of NRs during the deposition. As we cannot measure the mass deposited on the substrate *in situ* with our current setup, we measured the mass left on a similar substrate after immersing the substrate back to its solution at different time intervals without the applied voltage. Figure S3 shows one of the measurements. The curve can be fitted well by an exponentially decay function of $w = w_0 \exp\left(-\frac{t}{\tau_{dis}}\right)$, with $\tau_{dis} = 42 \pm 2\ s$.

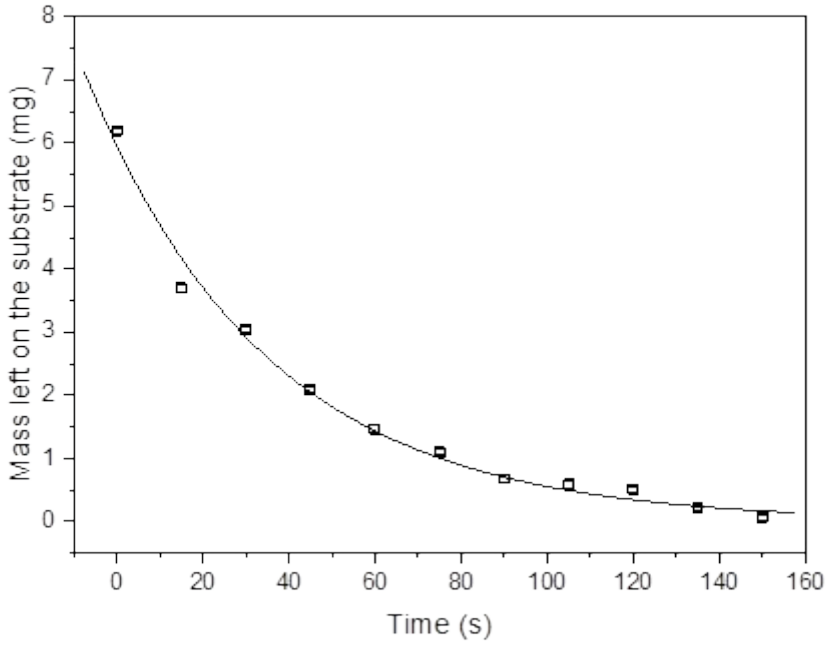


**Figure S3**: Dissolution measurement on the mass left on the substrate after immersing the sample into the NR solutions without external voltage. The solid line represents the exponential decay fit to the measured data.

It is worth noting that the dissolution time constant $\tau_{dis}$ can vary from one batch of NRs to another and is also sensitively dependent on the washing times of the NRs. It is more accurate to obtain the $\tau_{dis}$ for each batch of the NPs. From Figure S3, we can speculate that the dissolution rate in EPD is proportional to the mass deposited. We applied this relationship into eq. (6) of the main texts and obtained the analytical solution as shown in eq. (7) of the main texts. The thickness of the EPD samples can then be predicted using eq. (7). Eq. (S5) assumes that once the NPs re-dissolve back to its solution, they exist as neutral NPs.

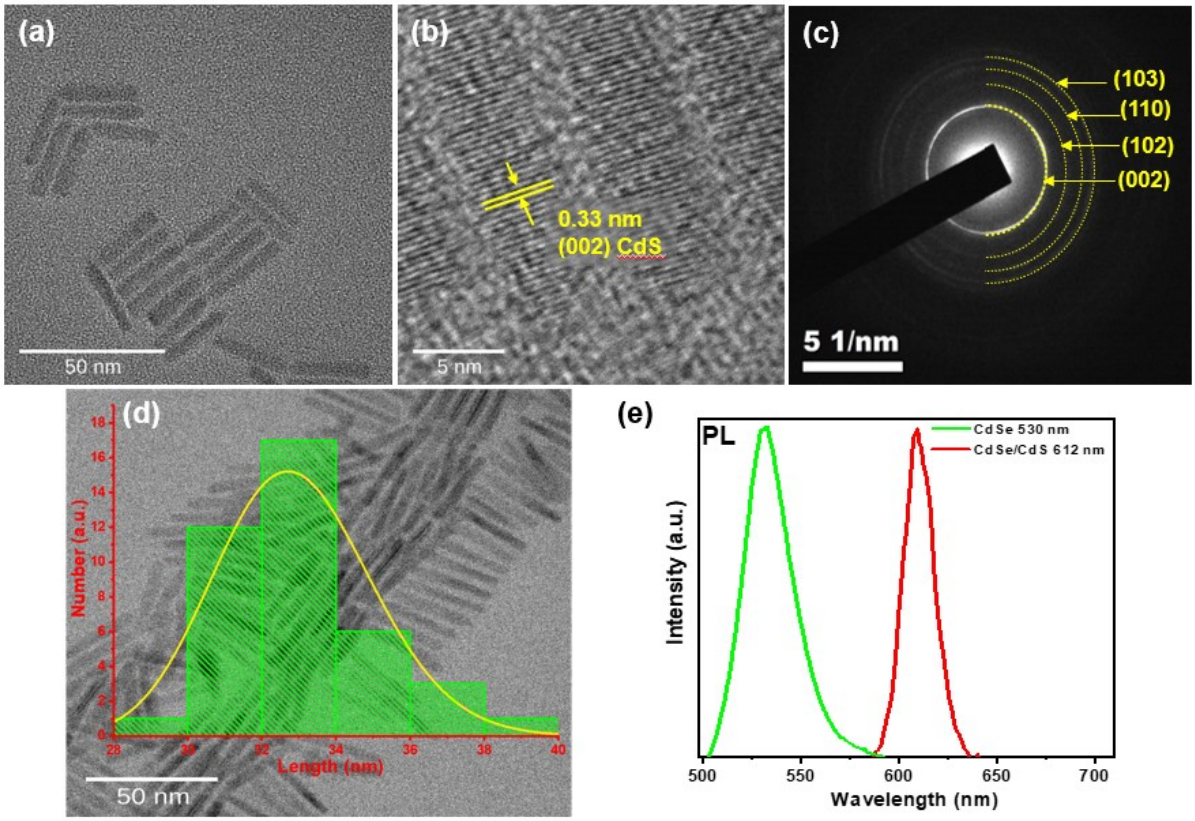


**Figure S4:** (a, b) Transmission electron microscopy images of CdSe/CdS core-shell nanorods (NRs). (c) Selected Area Electron Diffraction (SAED) pattern of the CdSe/CdS core-shell NRs. (d) Histogram of the length distribution of the NRs. (e) Photoluminescence of the CdSe core and CdSe/CdS core-shell NRs excited by a 405 nm CW laser.

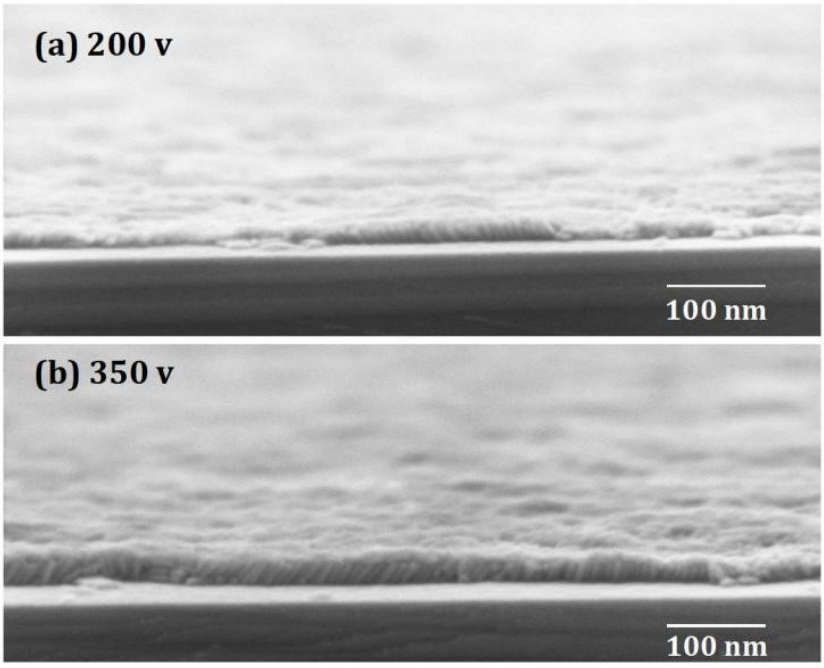


**Figure S5**: SEM cross section images of CdSe/CdS NR film on Si substrate after EPD from the NR solution (concentration 5 mg/ml) at (a) 200 V and (b) 350 V for 120 s, respectively.

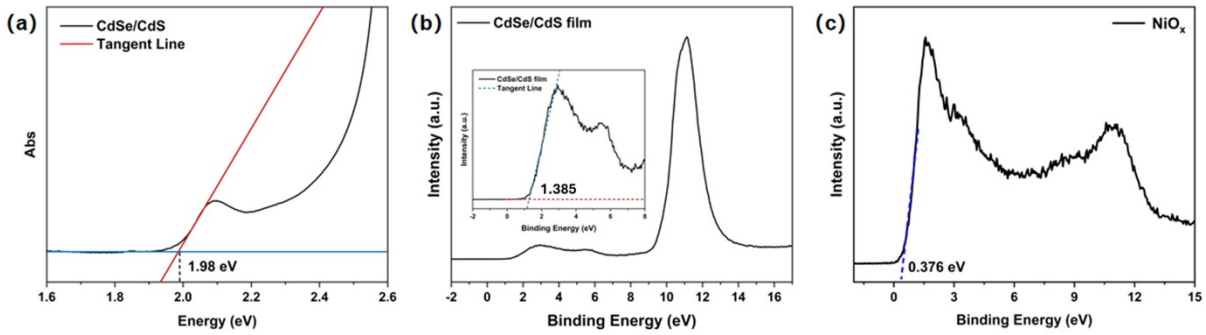


**Figure S6**: (a) UV-Vis absorption spectrum of CdSe/CdS NR film. (b, c) XPS valence band spectra of CdSe/CdS film and $NiO_x$ film respectively. The conduction and valence band positions of CdSe/CdS are obtained from these spectra.

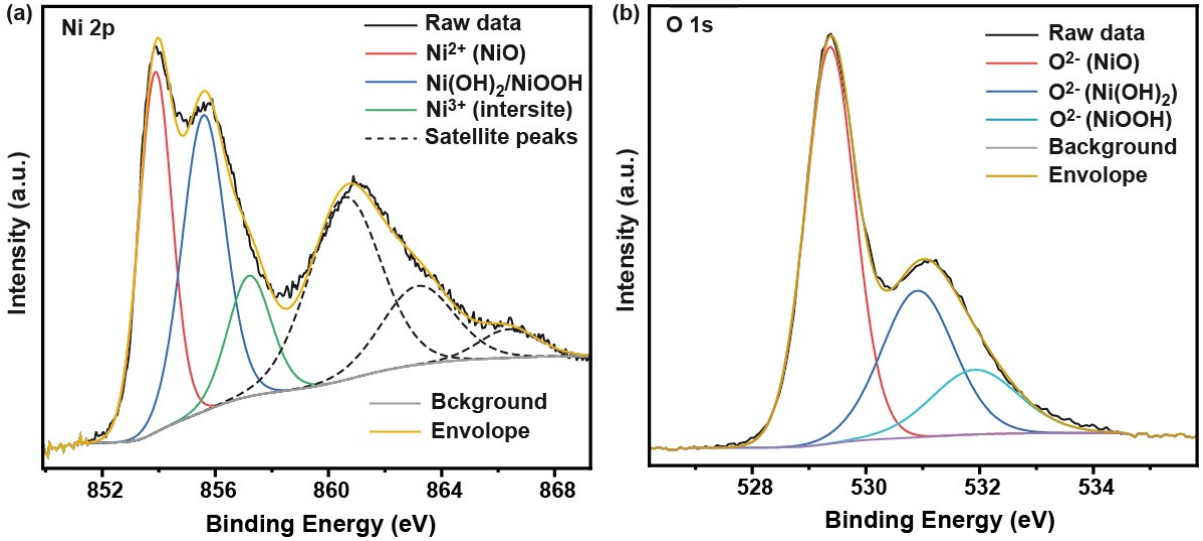


**Figure S7**: High resolution XPS of Ni 2p and O 1s states of $NiO_x$ deposited by reactive sputtering of Ni in $O_2$ followed by annealing.

Table S2: XPS analysis of $NiO_x$ deposited by reactive sputtering of Ni in $O_2$ followed by annealing

| | | ***$NiO_x$*** | |
|---|---|---|---|
| | | ***Conc. %*** | ***Position*** |
| ***Ni $2p_{3/2}$*** | $Ni^{2+}$(NiO) | 6.6 | 853.9 |
| | $Ni^{2+}$ ($Ni(OH)_2$)/$Ni^{3+}$ (NiOOH) | 7.0 | 855.6 |
| | $Ni^{3+}$ (Intersite) | 2.9 | 857.2 |
| ***O 1s*** | $O_\alpha$ (NiO) | 23.1 | 529.4 |
| | $O_\beta$ ($Ni(OH)_2$) | 12.4 | 530.9 |
| | $O_\gamma$ (NiOOH) | 6.6 | 531.9 |

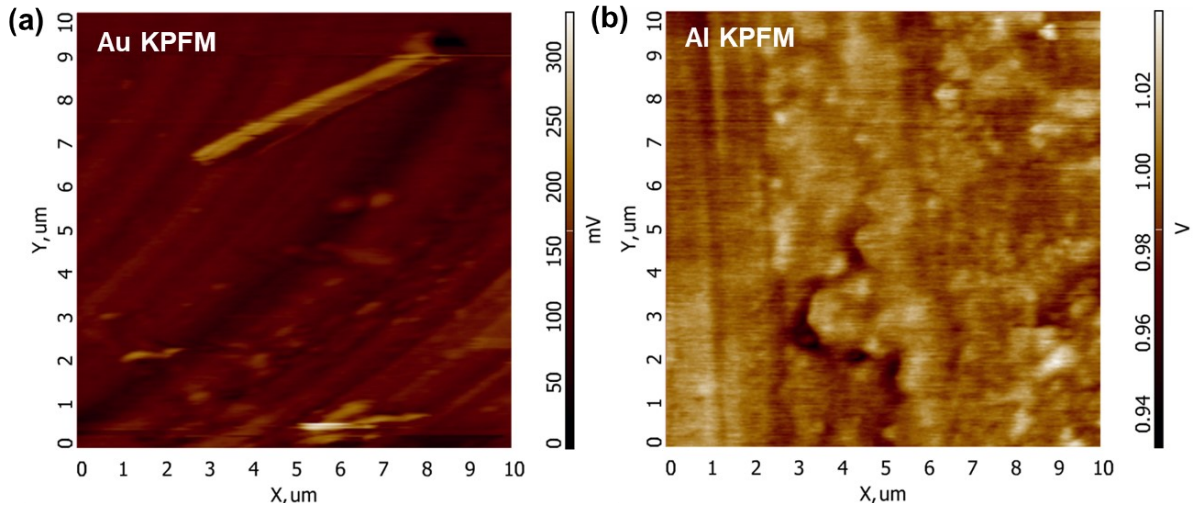


**Figure S8:** Kevin probe force microscopy images of calibration samples Au (a) and Al (b), respectively.

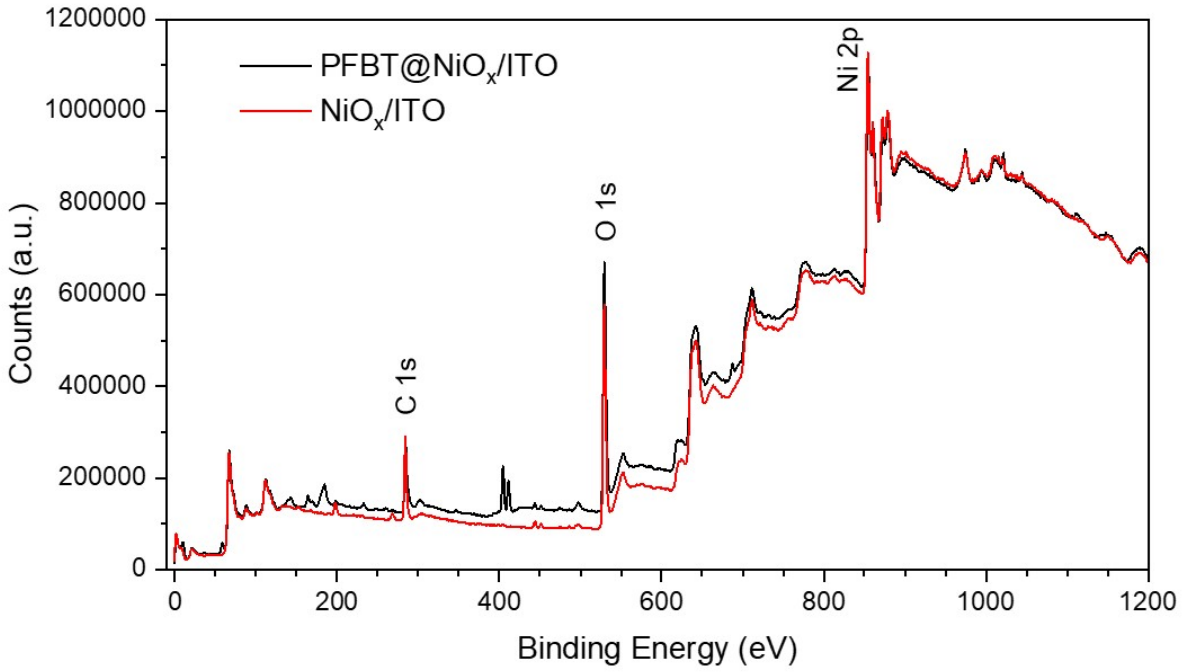


**Figure S9:** XPS survey scan on $NiO_x$/ITO film before and after PF-BT passivation

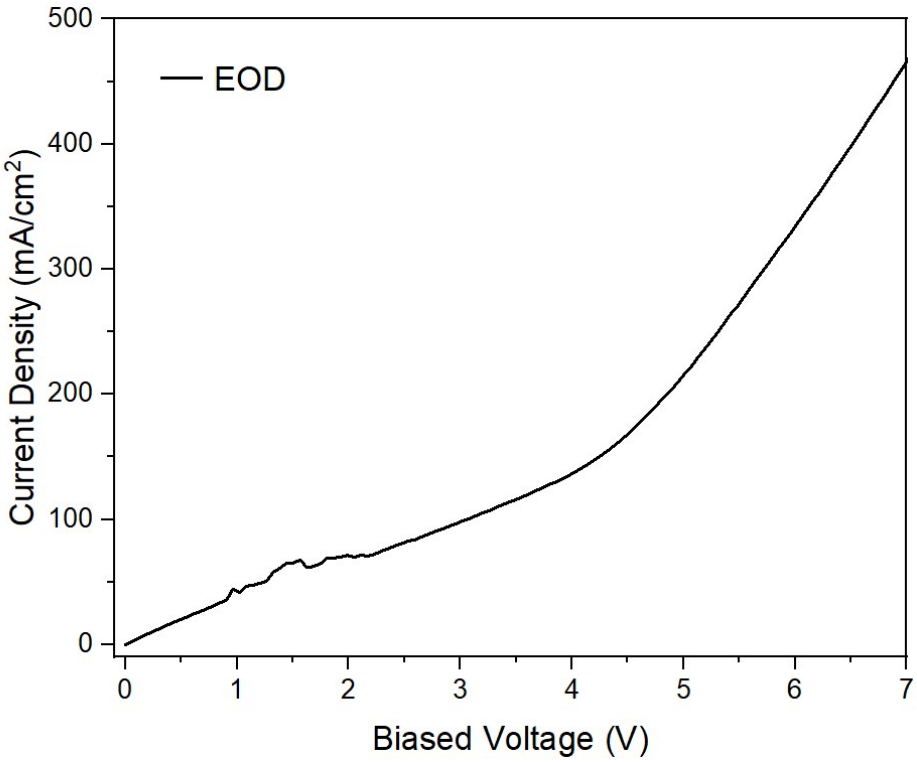


**Figure S10:** Current density vs. voltage measurement of an electron only device (EOD) with a similar configuration as shown in Figure 4(d), except $NiO_x$ was replaced by ZnMgO layer and no PF-BT layer was used in the structure.